Sarkar, Ritam; Bhunia, S.; Nag, D.; Barik, B. C.; Das Gupta, K.; Saha, D.; Ganguly, S.; Laha, Apurba; Lemettinen, Jori; Kauppinen, Christoffer; Kim, Iurii; Suihkonen, Sami; Gribisch, Philipp; Osten, Hans Jörg

Epi-Gd$_2$O$_3$/AlGaN/GaN MOS HEMT on 150 mm Si wafer: A fully epitaxial system for high power application

Epi-Gd$_2$O$_3$/AlGaN/GaN MOS HEMT on 150 mm Si wafer: A fully epitaxial system for high power application

Ritam Sarkar, S. Bhunia, D. Nag, B. C. Barik, K. Das Gupta (ID), D. Saha (ID), S. Ganguly (ID), Apurba Laha (ID), Jori Lemettinen (ID), Christoffer Kauppinen (ID), Iurii Kim (ID), Sami Suihkonen (ID), Philipp Gribisch, and Hans-Jörg Osten

View Online   Export Citation   CrossMark

ARTICLES YOU MAY BE INTERESTED IN

Control of the magnetic near-field pattern inside MRI machine with tunable metasurface
Applied Physics Letters **115**, 061604 (2019); https://doi.org/10.1063/1.5099413

Epitaxial growth and interface band alignment studies of all oxide α-Cr$_2$O$_3$/β-Ga$_2$O$_3$ p-n heterojunction
Applied Physics Letters **115**, 061602 (2019); https://doi.org/10.1063/1.5100589

Field-effect transistors with the three-dimensional Dirac semimetal cadmium arsenide
Applied Physics Letters **115**, 062101 (2019); https://doi.org/10.1063/1.5103268

Applied Physics Letters

Mid-IR and THz frequency combs
special collection

Read Now!

Epi-Gd₂O₃/AlGaN/GaN MOS HEMT on 150 mm Si wafer: A fully epitaxial system for high power application

Ritam Sarkar,[1] S. Bhunia,[2] D. Nag,[1] B. C. Barik,[2] K. Das Gupta,[2] (iD) D. Saha,[1] (iD) S. Ganguly,[1] (iD) Apurba Laha,[1,a)] (iD)
Jori Lemettinen,[3] (iD) Christoffer Kauppinen,[3] (iD) Iurii Kim,[3] (iD) Sami Suihkonen,[3] (iD) Philipp Gribisch,[4]
and Hans-Jörg Osten[4]

AFFILIATIONS

[1]Department of Electrical Engineering, Indian Institute of Technology Bombay, Mumbai 400076, India
[2]Department of Physics, Indian Institute of Technology Bombay, Mumbai 400076, India
[3]Department of Electronics and Nanoengineering, Aalto University, P. O. BOX 13500, FI-00076 AALTO, Finland
[4]Institute of Electronic Materials and Devices, Leibniz University Hannover, Schneiderberg 32, 30167 Hannover, Germany

[a)]Author to whom correspondence should be addressed: laha@ee.iitb.ac.in

ABSTRACT

In this letter, we report the impact of epitaxial Gd₂O₃ on the electrical properties of an AlGaN/GaN high electron mobility transistor (HEMT) grown on a 150 mm diameter Si (111) substrate. Incorporation of epitaxial Gd₂O₃ grown by the molecular beam epitaxy technique under a metal gate (metal/Gd₂O₃/AlGaN/GaN) causes six orders of magnitude reduction in gate leakage current compared to metal/AlGaN/GaN HEMT. We observe that epi-Gd₂O₃ undergoes complete structural changes from hexagonal to monoclinic as the thickness of the layer is increased from 2.8 nm to 15 nm. Such structural transformation is found to have a strong impact on electrical properties whereby the gate leakage current reaches its minimum value when the oxide thickness is 2.8 nm. We find a similar trend in the density of interface traps (D_{it}) having a minimum value of $2.98 \times 10^{12}\,\mathrm{cm}^{-2}\,\mathrm{eV}^{-1}$ for the epioxide layer of thickness 2.8 nm. Our measurements also confirm a significant increase in the two dimensional electron gas (2DEG) density (∼40%) at AlGaN/GaN interface with epioxide grown on AlGaN, thus confirming the contribution of epitaxial lattice strain on 2DEG modulation.

Published under license by AIP Publishing. https://doi.org/10.1063/1.5109861

The primary challenges that make a metal Schottky junction AlGaN/GaN high electron mobility transistor (HEMT) unreliable in high frequency, high power regions are junction degradation, high gate leakage,[1] and drain current collapse.[2] One of the most effective solutions to circumvent such practical challenges is to introduce an oxide beneath the metal and thus to realize a metal oxide semiconductor based HEMT, viz., MOSHEMT.[3] Several oxides including Al₂O₃,[4,5] HfO₂,[6] MgO,[7] Ga₂O₃,[8] Sc₂O₃,[9] and TiO₂[10] have been studied looking for an effective and plausible solution. In most of these studies, the oxides have been amorphous in nature. However, the fundamental limitation with these amorphous oxides is that they tend to become polycrystalline during post deposition high temperature treatments required for the device fabrication. Such a structural change often leads to high leakage current through oxides as the grain boundaries in polycrystalline oxide act as the percolation paths for charge leakage. Therefore, the thermal stability of those oxides at high temperature

has been one of the foremost challenging roadblocks to the practical application. However, if one replaces the amorphous oxide with a single crystalline epitaxial layer under gate, many of the above problems can be addressed without compromising other advantages. Since the oxide is already crystalline, it would withstand much higher temperature compared to that of an amorphous one.[3] Earlier reports on the epitaxial high-k dielectric on the GaN substrate have clearly demonstrated promising results.[11–14] The benefits of replacing amorphous oxide with an epitaxial oxide on the AlGaN/GaN heterostructure are threefold: (a) reduction of gate leakage current, (b) surface passivation of the AlGaN layer,[15] and (c) manipulation of two dimensional electron gas (2DEG) density by introducing additional strain in the AlGaN layer. Although most of the experiments reported so far dwell on the first advantage, we do not find any report on the 2DEG modulation with epitaxial oxide. In this work, we have studied the effect of ultrathin epitaxial Gd₂O₃ on gate leakage and 2DEG density of the

AlGaN/GaN heterostructure grown on a 150 mm Si (111) wafer. The oxide being single crystalline not only provides better thermal stability at high temperature but also exhibits a strong impact on the 2DEG density.

Furthermore, in order to address the challenges toward commercially viable large scale integration, the AlGaN/GaN heterostructure needs to be grown on a large area Si substrate. However, the large lattice mismatch between Si and GaN and strong difference in their thermal coefficient pose a formidable challenge when it comes to the context of epitaxial growth of GaN on Si. The large lattice mismatch creates a high density of misfit and threading dislocation (TD) in the AlGaN/GaN heterostructure, which severely degrades the electrical properties of 2DEG. In order to accommodate the tensile stress, minimize the dislocation related defects, and achieve a crack free GaN heterostructure, a wide variety of intermediate layers such as low temperature AlN,[16] graded AlGaN buffers,[17,18] and AlGaN/GaN super lattices[19] have been introduced between the GaN buffer and the Si substrate. In the present work, we used several layers of AlGaN with varying Al contents [shown in Fig. 1(a)] as the intermediate layer between GaN and Si substrates. Subsequently, we grow epitaxial Gd_2O_3 on an optimized AlGaN/GaN heterostructure in order to introduce an additional tensile strain into the AlGaN layer. We also present an in-depth structural and electrical characteristic of this fully epitaxial system. Our study shows that the gate leakage current is dropped by 6 orders of magnitude after introducing ultrathin ($\sim$2.8 nm) epi-Gd_2O_3 beneath the metal gate. Furthermore, we observe an increase in 2DEG density after introducing epitaxial ultrathin Gd_2O_3.

GaN (0001) layers were grown on 1 mm thick Si (111) wafers using the standard step graded AlGaN and AlN approach by the low pressure metal oxide vapor phase epitaxy (MOVPE) technique. The reactor has a 1×6-in. close coupled showerhead configuration. Trimethylaluminum (TMAl), trimethylgallium (TMGa), and ammonia (NH_3) were used as precursors for aluminum, gallium, and nitrogen, respectively. Hydrogen was used as the carrier gas. The heterostructure comprises an $\sim$300 nm AlN buffer, step graded AlGaN buffer with three different compositions ($\sim$300 nm $Al_{0.78}Ga_{0.22}N$, $\sim$300 nm $Al_{0.57}Ga_{0.43}N$, and $\sim$500 nm $Al_{0.27}Ga_{0.73}N$) and 1 μm GaN. This was followed by a 1.5 nm thick AlN layer, 26 nm thick $Al_{0.27}Ga_{0.73}N$, and 2 nm thick GaN cap layer.

Subsequently, we grew epi-Gd_2O_3 on an AlGaN/GaN virtual substrate in a multichamber solid source MBE system (DCA Instruments). Prior to the growth, the sample undergoes a thermal treatment at 650 °C for 30 min. The source material consists of granular Gd_2O_3, which was evaporated by electron beam heating.

The epioxide growth was performed at 650 °C with an average growth rate of 0.2 nm/min. Molecular oxygen was introduced in the growth chamber in order to maintain a partial pressure of 5 $\times 10^{-7}$ mbar during growth using a piezoleakage valve. This is essential to realize stoichiometric Gd_2O_3 because of oxygen depletion from the source material during evaporation. The thickness of the Gd_2O_3 layers was measured using the X-ray reflectometry (XRR) technique.

Figure 1(a) shows the cross-sectional scanning electron microscopy (SEM) image of the AlGaN/GaN heterostructure grown on the Si (111) substrate. All the layers such as an AlN layer followed by step graded multiple AlGaN layers are clearly evident in this figure. The cross-sectional SEM image further confirms the uniform thickness ($\sim$2.4–2.5 μm) across the 150 mm diameter of the Si (111) wafer. Figure 1(b) shows the actual picture of the 150 nm diameter Si (111) wafer with the AlGaN/GaN stack grown onto it.

In order to analyze the crystal quality and to estimate the Al content in the intermediate layers as well as the top AlGaN barrier layer, we have carried out the high resolution x-ray diffraction (HRXRD) measurement on these samples. Several diffraction peaks around the primary GaN (0002) peak are attributed to AlGaN intermediate layers with different Al contents. We further investigated the structure of epitaxial Gd_2O_3 by HRXRD. In order to identify the crystal phase of epi-Gd_2O_3, we performed the in-plane HRXRD measurement as peak positions of the (0002) and (-402) of reflections of bulk hexagonal and monoclinic Gd_2O_3, respectively in symmetric $2\theta/\square$ scan overlap each other.[12] We find that when the thickness of Gd_2O_3 increases from 2.8 nm to 15 nm, it undergoes a complete structural transformation from the hexagonal (H) to the monoclinic (M) phase, shown in Fig. 2(b). We also observe that intermediate 5.5 nm thick Gd_2O_3 exhibits a mixed phase structure (combination of M and H), which further infers the gradual phase transformation (from H to M) with the increase in the epi-Gd_2O_3 thickness. Earlier experiments[20] report a similar observation, i.e., epi-Gd_2O_3 with the thickness less than 4 nm exhibits a hexagonal structure, whereas the thicker layer (>6 nm) tends to have the monoclinic phase. Our in-plane measurement clearly depicts that for epi-Gd_2O_3 with a thickness of 15 nm, two distinct peaks, centered at $2\theta = 47.82°$ and $50.98°$, appear [shown in Fig. 2(b)].These peaks are attributed to the (3 ± 13) and (0 ± 20) planes of monoclinic Gd_2O_3.[20] Whereas, 5.5 nm thick Gd_2O_3 does show a broad peak with a shoulder inferring the presence of both hexagonal and monoclinic phases. However, for the case of 2.8 nm Gd_2O_3, the single peak appeared at $2\theta = 48.41°$, confirming the presence of the $(11\bar{2}0)$ plane which is attributed to H-Gd_2O_3 only.
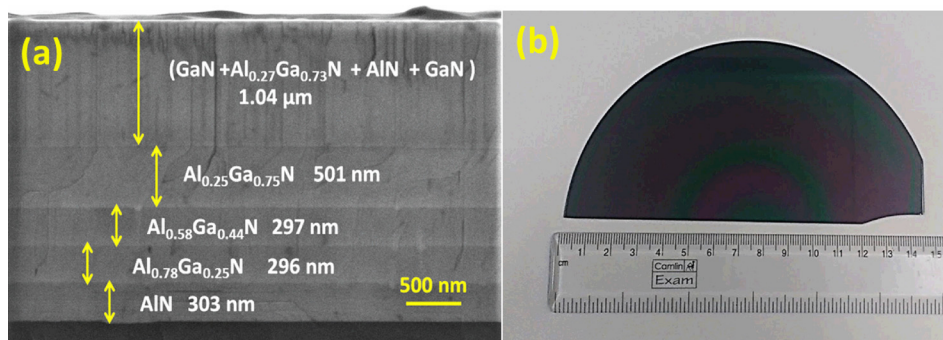

FIG. 1. (a) The cross-sectional SEM image of the AlGaN/GaN heterostructure grown on the 150 mm diameter Si wafer. (b) The picture of the 150 mm diameter wafer after epitaxial HEMT growth.
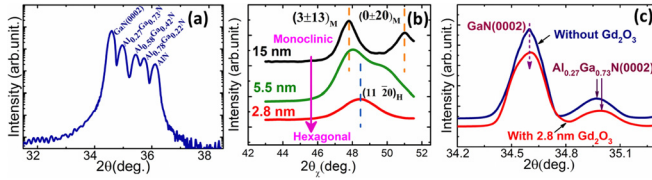
FIG. 2. (a) The HRXRD spectra of the symmetric $2\theta/\omega$ scan on the (0002) diffraction plane of the AlGaN/GaN heterostructure grown on the 150 mm Si (111) wafer. (b) The in-plane HRXRD scan of Gd_2O_3 grown on the AlGaN/GaN heterostructure which confirms the monoclinic (15 nm) to hexagonal (2.8 nm) phase transition of Gd_2O_3 with the reduction of oxide thickness. (c) The HRXRD spectra from the (0002) plane of GaN and AlGaN with and without Gd_2O_3 on top of the AlGaN/GaN heterostructure.

Further, for the sample with epioxide, we observe that the (0002) peak of the AlGaN barrier is shifted from $34.96° \pm 0.05°$ to $35.01° \pm 0.05°$ which implies the presence of compressive strain along the c-axis. The compression of the c-axis lattice constant occurs at the expense of in-plane tensile strain which is induced by the epitaxial oxide onto the AlGaN layer.

In order to estimate the electrical properties of the AlGaN/GaN heterostructure grown on 150 mm Si (111) wafer (which is the control sample), we performed one dimensional band diagram simulation of the AlGaN/GaN heterostructure using open source one dimensional Poisson, Drift-Diffusion, and Schrodinger Solver (1D–DDCC) software.[21] The electron concentration estimated for the present structure [shown in Fig. 3(a)] is around $1 \times 10^{19} cm^{-3}$. The 2DEG mobility and sheet carrier concentration are measured experimentally by the Hall effect measurement.

Figure 3(b) compares the sheet carrier concentration and 2DEG mobility measured at the different positions on the wafer (from the center to the edge along the diameter of 150 mm). As depicted in Fig. 3(c), the mobility remains within the range of $1400–1500 \, cm^2/V \, s$ across the wafer, with a similar trend in the sheet carrier concentration in the range of $5 \times 10^{12}–6 \times 10^{12} \, cm^{-2}$. The small variation in the mobility and electron concentration could be attributed to a minute fluctuation of Al concentration across the large diameter wafer. The surface morphology of the grown wafer has been analyzed by the
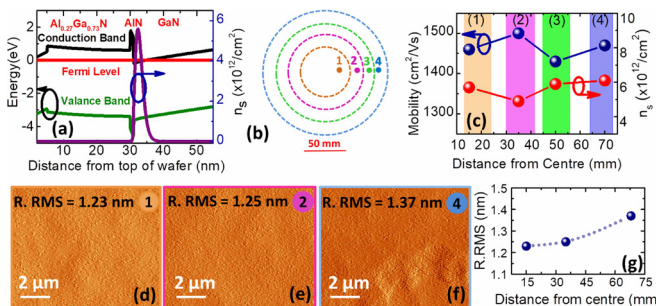
Atomic Force Microscopy (AFM) measurement. Figures 3(d)–3(f) show the AFM image at the center, middle, and edge of the wafer, respectively. As seen, the roughness of the layer remains uniform throughout the wafer. The average roughness measured within the $10 \times 10 \, \mu m$ scan area is around 1.2–1.3 nm [shown in Fig. 3(g)]. The slight increase in the surface roughness at the edge of the wafer may be attributed to the variation of the substrate temperature.

In order to study the electrical properties of the control sample AlGaN/AlN/GaN heterostructure without oxide, we fabricated the circular HEMT using the standard fabrication process. The source/drain ohmic contact comprises an electron beam evaporated Ti/Al/Ni/Au (30 nm/100 nm/30 nm/100 nm) layer. The lift-off process was followed by thermal annealing at 850 °C for 40 s in N_2. Finally, the gate electrode was prepared by depositing a Ni/Au (30 nm/100 nm) metal stack using electron beam heating. The measured sheet resistance of the source-drain is around $400 \, \Omega/\square$. Figure 4(a) shows the I_{ds}-V_{ds} and DC transfer characteristics of the AlGaN/AlN/GaN HEMT control sample. The maximum drain current measured is 175 mA/mm at $V_{GS} = 1 V$ and $V_{DS} = 4.5 V$. The relatively low drain saturation current compared to earlier reported results may be attributed to the large perimeter of the devices (source drain distance $\sim 20 \, \mu m$). The threshold voltage estimated from the transfer characteristic shown in Fig. 4(b) is around $-2.70 V$, and the maximum transconductance is 60 mS/mm. The I_{on}/I_{off} ratio of these devices is around 5×10^3 which is on par with recently reported results. We now evaluate the electrical characteristics of the AlGaN/GaN heterostructure with epitaxial Gd_3O_3 grown onto it. Tungsten metal was deposited through a shadow mask on epi-Gd_2O_3 for the gate contact.

One of the challenges with metal-Schottky junction AlGaN/GaN HEMT is the large gate leakage current at higher applied gate voltage because of the moderate conduction band offset between metal and AlGaN. The introduction of epitaxial Gd_2O_3 on the top of the AlGaN layer increases the conduction band offset which eventually reduces the gate leakage significantly. Figure 5(a) compares the leakage current measured on Gd_2O_3/AlGaN/AlN/GaN structures with varying oxide thicknesses. As is evident, the gate leakage is reduced by five orders of magnitude compared to the control AlGaN/AlN/GaN HEMT. The I-V plot in Fig. 5(a) shows that the leakage current value is $\sim 5 \times 10^{-8} \, A/cm^2$ at the gate voltage $V_G = -2 V$ with Gd_2O_3 of 5.5 nm. Excellent electrical properties of the Gd_2O_3/AlGaN/AlN/GaN structure endorse the advantage MOSHEMT which is further augmented by the epitaxial quality of oxide. Surprisingly, we observe that gate leakage turns out to be the minimum for 2.8 nm Gd_2O_3 and it reaches $\sim 4 \times 10^{-9} \, A/cm^2$ which is six times lower than that of the control device. We also observe that the leakage current starts increasing with the increase in the oxide thickness.

FIG. 3. (a) The simulated band diagram and electron concentration of the heterostructure. (b) The schematic diagram of the 150 mm diameter wafer, which indicates positions from the center to the edge. (c) The Hall measurement data of 2DEG mobility and sheet carrier concentration (n_s) from the center to the edge. (d)–(f) The ($10 \times 10 \, \mu m^2$) atomic force microscopy (AFM) images of the grown wafer surfaces at different positions. (g) The plot of surface roughness with the distance from the center of the sample wafer.
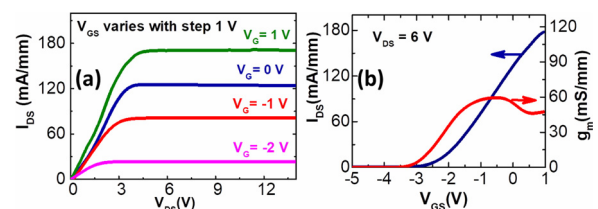

FIG. 4. (a) I_{DS} vs V_{DS} characteristics of the HEMT (control sample) grown on the 150 mm Si wafer. (b) The DC transfer characteristic of the control HEMT.
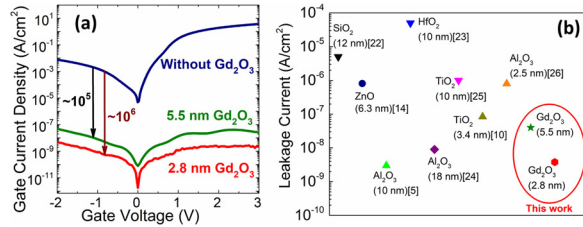
FIG. 5. (a) Gate leakage current (I_G) vs gate voltage (V_G) for control HEMT and MOSHEMT (2.8 nm and 5.5 nm) Gd_2O_3 thickness. (b) Comparison of the leakage current density of this work with earlier reported data on various dielectric-based MOS-HEMTs.

The contrary nature of the leakage current could be attributed to (a) phase transformation and presence of mixed phases in Gd_2O_3 (hexagonal to monoclinic) and (b) relaxation of the oxide layer beyond the critical thickness (~3 nm). Relaxation occurs as a result of formation of the misfit dislocation at the interface.[22] We further observe that the epioxide with a thickness of ~5.5 nm exhibits a mixed structure comprising both hexagonal (H) and monoclinic (M) phases [Fig. 2(b)]. This would lead to the formation of grains and grain-boundaries with individual grain possessing either H or M phase. Moreover, it was observed that the monoclinic phase of epi-Gd_2O_3 comprises several domains.[23] All these concomitant defects (grain and domain boundaries) eventually act as the leakage paths for the charge carriers, thus increasing the gate leakage current significantly. However, the ultrathin (~2.8 nm) pseudomorphically grown epi-Gd_2O_3 possesses a single phase (hexagonal) with no domain boundaries and hence behaves as an ideal oxide with no leakage path. The measured leakage current for this device turns out to be the lowest with its value as ~4×10^{-9} A/cm^2 at $V_G = -2$ V). We, therefore, conclude that ultrathin single crystal oxide with the thickness below the critical value would be the best suited oxide for MOSHEMT applications. The comparison between gate leakage current density and various dielectrics with different thicknesses[5,10,14,24–28] at the same gate voltage is shown in Fig. 5(b). Reference 5 reported the minimum leaking current density of 3×10^{-9} A/cm^2 which is comparable to our result (~4×10^{-9} A/cm^2).

In order to further evaluate the dielectric property of epi-Gd_2O_3, the capacitance-voltage (C-V) measurement was performed in different frequency ranges. Figure 6 shows the C-V curve of epi-G_2O_3 with two different thicknesses. The dielectric constant of Gd_2O_3 estimated from the C-V curve is around ~15. The interface trap density (D_{it}) has been calculated from the C-V curve at two different frequencies following the method derived in Ref. 29. We observe that the D_{it} value is reduced by one order of magnitude with the decrease in the oxide thickness. The minimum D_{it} measured is around ~2.98×10^{12} cm^{-2} eV^{-1} for the oxide thickness of 2.8 nm. The minimum D_{it} value of the thinnest oxide layer (2.8 nm) further affirms the impact of structural perfection as described earlier.

The effect of epitaxial oxide on 2DEG is measured by the van der Pauw based Hall measurement technique. In Fig. 7 (inset), it has been observed that the 2DEG is enhanced by 20% with 5.5 nm Gd_2O_3, which is primarily because of the presence of positive charge at the oxide/AlGaN interface. However, we observe the maximum increase in 2DEG (~40%) for the thinnest Gd_2O_3 of thickness 2.8 nm. We
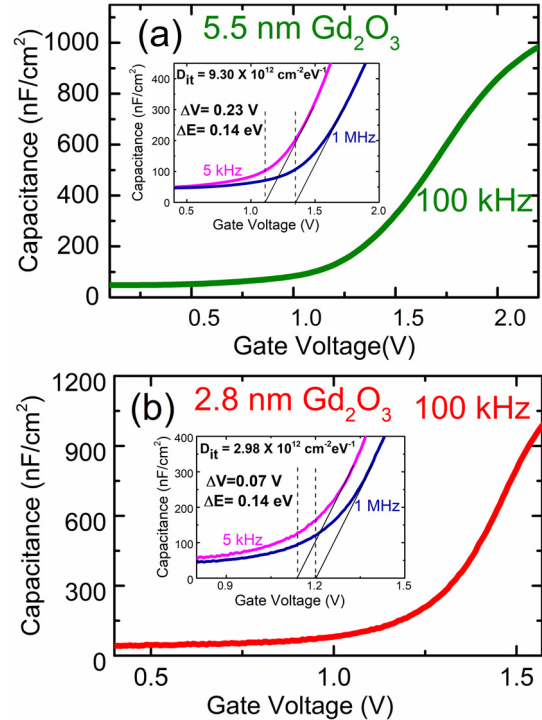

FIG. 6. (a) and (b) depict the C-V characteristics of MOSHEMT with two different thicknesses (5.5 nm and 2.8 nm) of Gd_2O_3 grown on the AlGaN/GaN heterostructure. The inset shows D_{it} calculated from the C-V curve on both cases.

attribute this enhancement of sheet carrier concentration to additional tensile strain in the AlGaN barrier induced by pseudomorphic Gd_2O_3. The excess electric field that stems from lattice strain increases the conduction band offset[30] which eventually enhances the 2DEG density. Simulating 2DEG properties with lattice strain and D_{it} being accounted for, we estimate a similar trend (shown in Fig. 7) as was measured using the Hall measurement. All our observations lead to
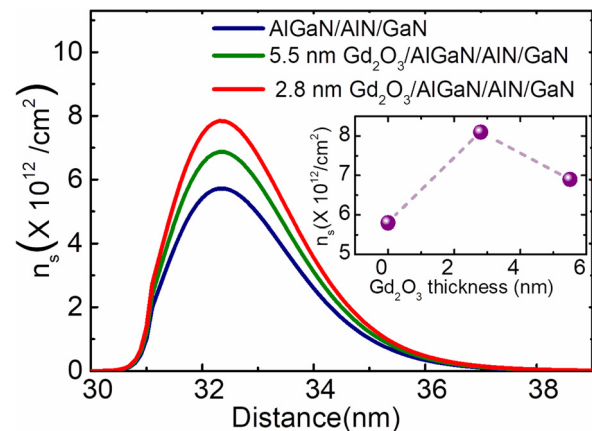

FIG. 7. shows the simulated and experimental (inset) evidence of the modulation of 2DEG density with the piezoelectric strain of Gd_2O_3.

the conclusion that modulation of strain in the AlGaN barrier is the most dominating feature impacting the 2DEG density at the AlGaN/GaN interface.

In summary, we demonstrate that epi-Gd_2O_3 not only reduces gate leakage current significantly but also improves the electrical properties of AlGaN/GaN HEMT by inducing additional strain in the AlGaN barrier. We further infer that in order to achieve the best performing MOSHEMT, we must optimize the structure and thickness of the oxide layer. The thickness of the epitaxial oxide layer must be kept under a critical value so as to achieve the best performance. We observe that epi-Gd_2O_3 if fully strained can also modulate the 2DEG density by modulating the tensile strain in the AlGaN barrier. Our experiments on all epitaxy MOSHEMT systems can pave the way for a commercially viable and radical solution for future nitride based high frequency and high power devices. We believe that epi-Gd_2O_3/AlGaN/GaN indeed holds huge potential and tremendous promise for high power and high frequency applications in years to come.

REFERENCES

[1] J. W. Chung, J. C. Roberts, E. L. Piner, and T. Palacios, IEEE Electron Device Lett. **29**, 1196 (2008).

[2] T. Mizutani, Y. Ohno, M. Akita, S. Kishimoto, and K. Maezawa, IEEE Trans. Electron Devices **50**, 2015 (2003).

[3] Z. Gao, M. F. Romero, A. Pampillon, E. S. Andres, and F. Calle, IEEE Trans. Electron Devices **63**, 2729 (2016).

[4] Q. Wu, D. Y. Ye, D. P. Wilk, and B. G. Yang, Mater. Sci. Eng., B **135**, 282–284 (2006).

[5] S. Huang, S. Yang, J. Roberts, and K. J. Chen, Jpn. J. Appl. Phys. **50**, 110202 (2011).

[6] Y. Yue, Y. Hao, J. Zhang, J. Ni, W. Mao, Q. Feng, and L. Liu, IEEE Electron Device Lett. **29**, 838 (2008).

[7] J. Kim, R. Mehandru, B. Luo, F. Ren, B. P. Gila, A. H. Onstine, C. R. Abernathy, S. J. Pearton, and Y. Irokawa, Appl. Phys. Lett. **80**, 4555 (2002).

[8] C. T. Lee, H. W. Chen, and H. Y. Lee, Appl. Phys. Lett. **82**, 4304 (2003).

[9] R. Mehandru, B. Luo, J. Kim, F. Ren, B. P. Gila, A. H. Onstine, C. R. Abernathy, S. J. Pearton, D. Gotthold, R. Birkhahn, B. Peres, R. Fitch, J. Gillespie, T. Jenkins, J. Sewell, D. Via, and A. Crespo, Appl. Phys. Lett. **82**, 2530 (2003).

[10] A. Rawat, M. Meer, V. K. Surana, N. Bharadwaj, V. Pendem, N. Garigapati, S. Ganguly, and D. Saha, IEEE Trans. Electron Devices **65**, 3725 (2018).

[11] Y. C. Chang, Y. J. Lee, Y. N. Chiu, T. D. Lin, S. Y. Wu, H. C. Chiu, J. Kwo, Y. H. Wang, and M. Hong, J. Cryst. Growth **301–302**, 390 (2007).

[12] W. H. Chang, C. H. Lee, P. Chang, Y. C. Chang, Y. J. Lee, J. Kwo, C. C. Tsai, J. M. Hong, C. H. Hsu, and M. Hong, J. Cryst. Growth **311**, 2183 (2009).

[13] W. H. Chang, C. H. Lee, Y. C. Chang, P. Chang, M. L. Haung, Y. J. Lee, C. H. Hsu, J. M. Hong, C. C. Tsai, J. R. Kwo, and M. Hong, Adv. Mater. **21**, 4970 (2009).

[14] S. Yoon, S. Lee, H. S. Kim, H. Y. Cha, H. D. Lee, and J. Oh, Semicond. Sci. Technol. **33**, 015007 (2018).

[15] C. Liu, E. F. Chor, and L. S. Tan, Semicond. Sci. Technol. **22**, 522 (2007).

[16] A. Dadger, J. Blasing, A. Diez, A. Alam, M. Heuken, and A. Krost, Jpn. J. Appl. Phys., Part 2 **39**, L1183 (2000).

[17] H. Ishikawa, G. Y. Zhao, N. Nakada, T. Egawa, T. Jimbo, and M. Umeno, Jpn. J. Appl. Phys., Part 2 **38**, L492 (1999).

[18] H. Marchand, L. Zhao, N. Zhang, B. Moran, R. Coffie, U. K. Misra, J. S. Speak, S. P. DenBaars, and J. A. Freitas, J. Appl. Phys. **89**, 7846 (2001).

[19] E. Feltin, B. Beaumont, M. Laügt, P. de Mierry, P. Vennéguès, H. Lahrèche, M. Leroux, and P. Gibart, Appl. Phys. Lett. **79**, 3230 (2001).

[20] W. H. Chang, S. Y. Wu, C. H. Lee, T. Y. Lai, Y. J. Lee, P. Chang, C. H. Hsu, T. S. Huang, J. R. Kwo, and M. Hong, ACS Appl. Mater. Interfaces **5**, 1436 (2013).

[21] H. H. Cheng, J. S. Speck, C. Weisbuch, and Y. R. Wu, Appl. Phys. Lett. **113**, 153504 (2018).

[22] L. Dong, J. Schnitker, R. W. Smith, and D. J. Srolovitz, J. Appl. Phys. **83**, 217 (1998).

[23] W. H. Chang, P. Chang, T. Y. Lai, Y. J. Lee, J. Kwo, C. H. Hsu, and M. Hong, Cryst. Growth Des. **10**, 5117 (2010).

[24] S. Arulkumaran, T. Egawa, H. Ishikawa, and T. Jimbo, Appl. Phys. Lett. **84**, 613 (2004).

[25] A. Kawano, S. Kishimoto, Y. Ohno, K. Maezawa, T. Mizutani, H. Ueno, T. Ueda, and T. Tanaka, Phys. Status Solidi C **4**, 2700 (2007).

[26] C. Mizue, Y. Hori, M. Miczek, and T. Hashizume, Jpn. J. Appl. Phys., Part 1 **50**, 021001 (2011).

[27] H. Y. Liu, C. S. Lee, W. C. Hsu, T. T. Wu, H. S. Huang, S. F. Chen, Y. C. Yang, B. C. Chiang, and H. C. Chang, in Proceedings of IEEE 11th International Conference on Power Electronics and Drive Systems (2015), p. 578.

[28] K. Takhar, B. B. Upadhyay, Y. K. Yadav, S. Ganguly, and D. Saha, Appl. Surf. Sci. **481**, 219 (2019).

[29] Y. Hori, Z. Yatabe, and T. Hasizume, J. Appl. Phys. **114**, 244503 (2013).

[30] Y. Zhang and J. Singh, J. Appl. Phys. **85**, 587 (1999).